SCIENCE CHINA
Technological Sciences

•Article•

https://doi.org/10.1007/s11431-020-1732-5

Liquid vaporization under thermodynamic phase non-equilibrium condition at the gas-liquid interface

WANG XingJian[1*], LAFON Patrick[2], SUNDARAM Dilip[3] & YANG Vigor[3*]

[1] *Department of Mechanical and Civil Engineering, Florida Institute of Technology, Melbourne, Florida 32901, USA;*
[2] *Department of Mechanical and Nuclear Engineering, The Pennsylvania State University, University Park, PA 16802, USA;*
[3] *School of Aerospace Engineering, Georgia Institute of Technology, Atlanta, GA 30332, USA*

Received September 8, 2020; accepted September 25, 2020; published online November 9, 2020

Liquid vaporization under thermodynamic phase non-equilibrium condition at the gas-liquid interface is investigated over a wide range of fluid state typical of many liquid-fueled energy conversion systems. The validity of the phase-equilibrium assumption commonly used in the existing study of liquid vaporization is examined using molecular dynamics theories. The interfacial mass flow rates on both sides of the liquid surface are compared to the net vaporization rate through an order-of-magnitude analysis. Results indicated that the phase-equilibrium assumption holds valid at relatively high pressures and low temperatures, and for droplets with relatively large initial diameters (for example, larger than 10 μm for vaporizing oxygen droplets in gaseous hydrogen in the pressure range from 10 atm to the oxygen critical state). Droplet vaporization under superheated conditions is also explored using classical binary homogeneous nucleation theory, in conjunction with a real-fluid equation of state. It is found that the bubble nucleation rate is very sensitive to changes in saturation ratio and pressure; it increases by several orders of magnitude when either the saturation ratio or the pressure is slightly increased. The kinetic limit of saturation ratio decreases with increasing pressure, leading to reduced difference between saturation and superheat conditions. As a result, the influence of non-equilibrium conditions on droplet vaporization is lower at a higher pressure.

liquid vaporization, droplet vaporization, superheated vaporization, thermodynamic phase equilibrium, thermodynamic phase non-equilibrium, vapor nucleation

Citation: Wang X J, Lafon P, Sundaram D, et al. Liquid vaporization under thermodynamic phase non-equilibrium condition at the gas-liquid interface. Sci China Tech Sci, 2020, 63, https://doi.org/10.1007/s11431-020-1732-5

1 Introduction

Vaporization of liquid droplets is a common phenomenon in nature and engineering applications, such as spray drying, fire suppression, and energy conversion for propulsion and power-generation systems [1]. In combustion devices, liquid fuel is injected and breaks up into small droplets through atomization, which then undergo a sequence of vaporization, mixing, and chemical reactions. The modeling of droplet vaporization and combustion has been extensively studied and the state of the art has been summarized in numerous reviews [2–6]. As noted by Sazhin [6], most existing models for vaporization were developed for thermodynamic sub-critical conditions. In many practical systems, chamber pressures and temperatures may approach or even exceed the thermodynamic critical states of injected fluids [7]. Several studies have been conducted to understand droplet vaporization at high pressures in quiescent [8–13] and convective environments [14–16]. The formulation requires detailed treatment of general-fluid thermodynamics and transport [7].

In the modeling of droplet vaporization, thermodynamic phase equilibrium is usually assumed to prevail at the liquid-gas interface. Such assumption significantly simplifies the analysis and leads to the classic D^2-law (D is droplet dia-

---

*Corresponding authors (email: wangx@fit.edu; vigor.yang@aerospace.gatech.edu)

meter) model [17]. The liquid-phase temperature is treated as uniformly distributed at a wet-bulb value; the vapor mass fraction at the interface is determined by the Clausius-Clapeyron relation. Numerous droplet vaporization models based on the D^2-law model have been proposed to improve spray calculations. Aggarwal et al. [18] evaluated several models for isolated droplets and sprays, including the D^2-law, infinite conductivity, diffusion limit, and internal vortex circulation models. Abramzon and Sirignano [19] developed a comprehensive vaporization model incorporating the effects of variable thermophysical properties, non-unit Lewis number, Stefan flow on heat and mass transfer between two phases, internal circulation, and transient liquid heating. These models, although at different levels of complexity, all rely on the assumption of thermodynamic phase equilibrium at the droplet surface. This implies that the mass fluxes of liquid and vapor molecules crossing the interface are several orders of magnitude greater than the net vaporization rate of the droplet. In other words, the characteristic time of achieving phase equilibrium is at least several orders of magnitude shorter than the diffusion times governing droplet vaporization. It is questionable whether this assumption is always valid, and it should be investigated under a range of operating conditions.

The effect of thermodynamic non-equilibrium on liquid droplet vaporization is not well understood. Miller et al. [20] calculated the vaporization rates of hydrocarbons and water droplets of diameter ~1 mm at atmospheric pressure using both equilibrium and non-equilibrium models. The non-equilibrium effects were treated using the Langmuir-Knudsen law. Results suggested that non-equilibrium effects are important both for droplets with diameters smaller than 50 μm and when gas temperatures are at or above the boiling point. Dahms and Oefelein [21] recently studied non-equilibrium gas-liquid interfacial dynamics in high-pressure liquid injection systems. Emphasis was placed on understanding of the transition from classical spray atomization to single-phase continuous dense-fluid mixing. At supercritical conditions, the interfacial layer was predicted to be much wider than the mean-free-path of the molecules, and deviations from the vapor-liquid equilibrium condition were substantial. The transition process was dictated by the statistical fluctuations of interface molecule numbers and the presence of interfacial forces. The interfacial free energy forces did not instantly diminish, but decreased gradually as the interface deteriorated. Furthermore, the interfacial region supported the development of thermal gradients.

Non-equilibrium vaporization and condensation processes at the liquid-vapor interface have been studied using kinetic modeling and molecular dynamic (MD) simulations. Sazhin et al. [22] developed a kinetic model for droplet vaporization in a high-pressure gaseous environment. The droplet surface is divided into two regions: a kinetic region that is modeled using the Boltzmann equation, and a hydrodynamic region. In the immediate vicinity of the droplet surface, Boltzmann equations were used to study vapor and gas dynamics, while hydrodynamic equations were used for analysis away from the surface. The challenge arose at the boundary of the kinetic and hydrodynamic regions, where self-consistent heat and mass fluxes were required [23]. Librovich et al. [24] developed a mathematical model for vaporization and condensation rates by means of kinetic theories to study ammonia-water systems with various initial conditions. The model was designed to treat situations with and without boiling. Xie et al. [25] performed MD simulations of *n*-dodecane vaporization and condensation. They found that large translational energy is necessary for molecules to evaporate and condense across the interface, and that the velocity distribution functions of molecules in the interfacial region are close to be isotropic Maxwellian for all velocity components. Xiao et al. [26] explored the vaporization processes of an *n*-dodecane droplet in both sub- and super-critical nitrogen environments using MD simulations. A regime diagram describing the vaporization modes was obtained as a function of ambient pressure, temperature, and initial droplet size.

The present study focuses on liquid vaporization under thermodynamic non-equilibrium conditions at pressure levels typical of the operating conditions of many propulsion and power-generation systems. The validity of the phase equilibrium assumption is first examined from an MD viewpoint by comparing interfacial molecular mass flow rates and the net vaporization rate of the droplet. As a specific example, calculations are performed for an oxygen/hydrogen system, which is commonly used in cryogenic energy-conversion devices. Qualitatively similar results are expected for hydrocarbon/oxygen systems. The pressure range of concern is 10–50 atm and the ambient temperature is varied in the range of 1000–2500 K. We then estimate the limit of non-equilibrium conditions from the perspectives of both thermodynamic stability and kinetic outlooks. In addition, we study the vaporization of the liquid droplet under superheated conditions. Both thermodynamic modeling and MD theory are used to analyze the stability of the liquid metastable phase. The classical binary nucleation theory, in conjunction with a real-fluid equation of state, is employed to analyze homogeneous nucleation of the binary system. The influence of non-equilibrium conditions on the droplet vaporization rate and lifetime is discussed.

2 Validity of phase equilibrium assumption

The liquid and vapor phases of the fluid are separated by an interfacial region, as shown in Figure 1. The thickness of the interfacial region is on the order of the mean-free-path of the

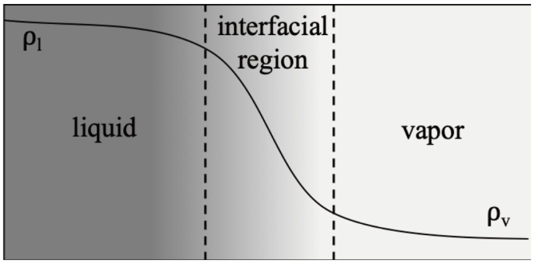

Figure 1 Schematic of interface between liquid and vapor phases of a fluid.

molecules. To a good approximation, the interfacial region can be approximated as a surface, marked by an abrupt change in the density of the fluid. The flux of molecules crossing the interface from one bulk phase to the other is estimated, that is, the mass flux from the liquid to the gas phase is denoted as vaporization rate, and the mass flux from the gas to the liquid phase is as condensation rate. The net vaporization rate is the difference between the two fluxes. A dynamic equilibrium is achieved when the flux of vapor molecules across the interface is balanced by its liquid counterpart.

The surface of a vaporizing droplet is typically assumed to be in thermodynamic phase equilibrium. The approximation is evaluated by comparing the mass fluxes of liquid and vapor molecules crossing the interface and the net vaporization rate of the droplet. The molecular distribution function in the liquid-vapor interfacial region is assumed to be isotropic Maxwellian, with the temperature equal to that of the liquid phase without drift velocity [25]. The maximum molecular flux density of molecules, j, from the vapor to liquid phase across the interface is calculated as follows [27]:

$$j_{N_i} = \frac{1}{4}\left(\frac{N_i}{V}\right)\sqrt{\left(\frac{8k_{\mathrm{B}}T}{\pi m_i}\right)}, \tag{1}$$

where N_i is the number of molecules, V is the volume, k_{B} is the Boltzmann's constant, T is the liquid surface temperature, and m is the mass of molecule i. After rearrangement, eq. (1) can be expressed in the following form:

$$j_{N_i} = \frac{\rho X_i}{W}\left(\frac{R_{\mathrm{u}}T}{2\pi W_i}\right)^{1/2} N_{\mathrm{A}}^{-1}, \tag{2}$$

where N_{A}, ρ, R_{u}, and X_i are the Avogadro number, mixture density, universal gas constant, and mole fraction of species i, respectively. Note that the actual vaporization rate (molecular flux density of evaporated molecules) and condensation rate (molecular flux density of condensed molecules) are lower than j_{N_i}, because of the reflection of vapor and liquid molecules on both sides of the interface surface. They are determined according to the corresponding vaporization and condensation coefficients (also known as mass accommodation coefficient). Molecular dynamics simulations have been performed to determine mass accommodation coefficient and its variation under different pressures and temperatures [28,29]. In the present analysis, the vaporization and condensation coefficients are set to unity [22]. The molecular flux density in eq. (2) is used for direct comparison with the net vaporization rate. The ratios of the interfacial mass flow rates to the net vaporization rate of the droplet (M_i^{l} and M_i^{v}) are given respectively by

$$\begin{aligned} M_i^{\mathrm{l}} &= \frac{(m_i A_s j_{N_i})^{\mathrm{l}}}{\dot{m}_{i,\mathrm{vap}}}, \\ M_i^{\mathrm{v}} &= \frac{(m_i A_s j_{N_i})^{\mathrm{v}}}{\dot{m}_{i,\mathrm{vap}}}, \end{aligned} \tag{3}$$

where superscripts l and v denote the mass flow rate across the interface from the bulk liquid phase (vaporization) and gaseous phase (condensation), respectively; A_s represents the interfacial area and $\dot{m}_{i,\mathrm{vap}}$ is the net vaporization mass flow rate of species i. As an example, calculations are performed for a liquid oxygen droplet in gaseuos hydrogen. The net vaporization rate under equilibrium conditions is obtained via one-dimensional numerical simulations of droplet vaporization. Detailed descriptions of the model are presented in ref. [13].

Figure 2 shows the temporal variation of M for a 100 μm liquid oxygen droplet at 100 K in a hydrogen environment at a pressure of 30 atm and a temperature of 1000 K. The interfacial mass flow rate for hydrogen is at least four orders of magnitude greater than the net vaporization rate. This indicates that hydrogen transfer at the interface is not a limiting factor in the achievement of thermodynamic equilibrium. A singular point appears in both curves of hydrogen due to the directional change of the net mass flow rate. The gaseous hydrogen initially condenses and aggregates within the liquid droplet. Then the trend is reversed as the hydrogen vaporizes. For oxygen, the ratio is slightly more than 3. Phase equilibrium is thus a reasonable approximation at the

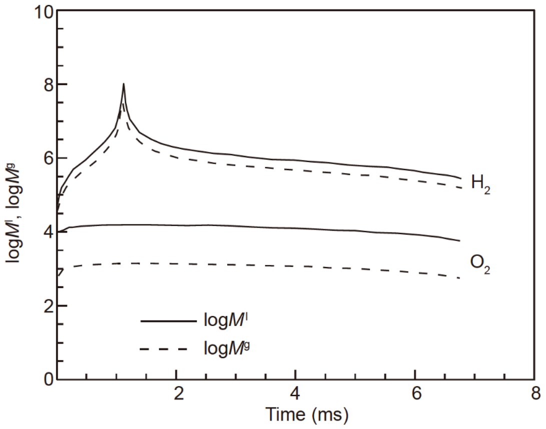

Figure 2 Temporal variation of the parameter M for an initial diameter D=100 μm liquid oxygen droplet at 100 K in a hydrogen environment at a pressure of 30 atm and temperature of 1000 K.

liquid-gas interface for oxygen-hydrogen systems under the given condition. For both oxygen and hydrogen, the ratio for vaporization is higher than that for condensation, mainly because of the density difference between the liquid and gaseous phases when evaluating mass flux density.

Lafon et al. [13] found that the droplet surface regression rate approximately follows the result of classic D^2-law at subcritical pressures. The droplet lifetime is proportional to the square of the initial droplet diameter. The net vaporization mass flow rate is linearly proportional to droplet diameter. In such equilibrium vaporization regime, the droplet surface temperature reaches a constant value after the heat-up period, so does the interfacial composition. It is apparent from eq. (3) that the interfacial mass flow rate is a quadratic function of the droplet diameter. As a result, the order of magnitude of the parameter M is reduced by one if the initial diameter is decreased by a factor of 10, which implies that $M_{\mathrm{O}_2}^{\mathrm{v}}$ is on the order of 100 for a droplet diameter of 10 μm at the same temperature and pressure as in Figure 2. The phase equilibrium assumption thus becomes questionable for droplets smaller than 10 μm.

The pressure and temperature of the ambient gas are two other parameters that dictate the conditions at the droplet surface. Figures 3 and 4 show the effects of ambient pressure and temperature on the parameter $M_{\mathrm{O}_2}^{\mathrm{v}}$ (the smallest of the four ratios in Figure 2) for a 100 μm liquid oxygen droplet in gaseous hydrogen. The pressure varies in the range of 10–50 atm and the ambient temperature in the range of 1000–2500 K. The order of magnitude of $M_{\mathrm{O}_2}^{\mathrm{v}}$ is marginally affected by changes in the ambient conditions, and it rises slightly from below 3 to above 3 as the pressure increases from 10 to 50 atm. This phenomenon can be explained by the fact that the net vaporization rate of the droplet is a weak function of pressure while the flux of vapor molecules across the interface is directly proportional to pressure. The assumption of phase equilibrium at the droplet surface is thus more valid at higher pressures. Ambient temperature exerts a substantial effect on the behavior of droplet vaporization. For example, the droplet lifetime decreases from about 7 ms at 1000 K to 3.5 ms at 2500 K. As a result, non-equilibrium effects are more important at higher ambient temperatures. This trend is consistent with the results of Miller et al. [20] for 2 mm decane droplets at 1 atm pressure.

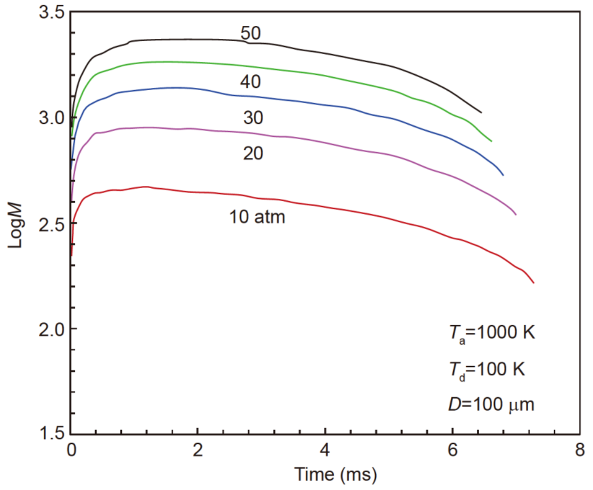

Figure 3 (Color online) Effect of pressure p_a on the parameter M for an initial diameter D=100 μm liquid oxygen droplet in a hydrogen environment at ambient temperature T_a=1000 K.

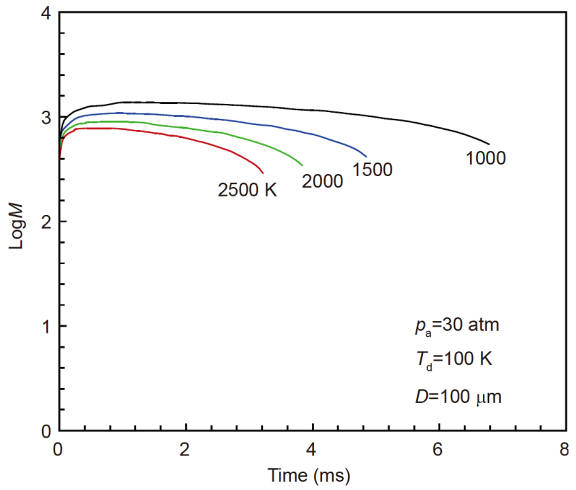

Figure 4 (Color online) Effect of ambient temperature T_a on the parameter M for an initial diameter D=100 μm liquid oxygen droplet in a hydrogen environment at ambient pressure p_a=30 atm.

This order-of-magnitude analysis shows that the thermodynamic equilibrium assumption is valid for oxygen droplets vaporizing in gaseous hydrogen, as long as the droplet initial diameter is above a threshold value close to 10 μm. The atomized droplet diameter in propulsion engines is usually about 100 μm, and the threshold value of droplet diameter is reached when 99% of the droplet mass is vaporized, rendering negligible impact in equilibrium calculations.

It is important to mention the uncertainties concerning the present analysis. The molecular distribution function is here assumed to be isotropic Maxwellian, and unity vaporization and condensation coefficients are used. Deviations from this distribution function and non-unity coefficients may be expected [25]. These effects can be incorporated into a more complete model in the future.

3 Droplet vaporization under superheated conditions

Vaporization of liquid droplets may not always occur under equilibrium conditions. As discussed in Section 2, the assumption of phase equilibrium becomes questionable at high ambient temperatures. In some cases, the liquid droplet does not vaporize until it is heated to above the equilibrium boiling temperature (saturation temperature). Superheating can be achieved when a liquid droplet, free of nucleation sites such as impurities, is heated suddenly to a temperature above its boiling point without boiling, and vice versa for supercooled vapor. The most important parameter characterizing droplet vaporization under phase non-equilibrium conditions is the rate of nucleation of the vapor phase. Assuming constant temperature and pressure, the droplet undergoes transformation such that the Gibb's free energy is minimized. Under superheated condition, the Gibb's free energy of the liquid phase is greater than that of the vapor phase. This provides the driving force for the vaporization process under phase non-equilibrium conditions. The formation of the vapor bubble inside a liquid droplet must overcome the surface tension force. The Gibb's free energy change, ΔG, can thus be expressed as [30]

$$\Delta G = (g_{\mathrm{v}} - g_{\mathrm{l}})V_{\mathrm{b}} + \sigma A_{\mathrm{b}}, \tag{4}$$

where g is the Gibb's free energy per unit volume, V_{b} is the bubble volume, A_{b} is the surface area of the bubble, and σ is the surface tension. The subscripts v and l refer to vapor and liquid phases, respectively. For bubbles with diameters lower than a critical value, the Gibb's free energy change is negative. The bubble can continue to grow only when its diameter is greater than a critical value. In classical homogeneous-homomolecular nucleation theory [30], the nucleation rate, J, can be written in the form:

$$J = K\exp\left(-\frac{\Delta G^*}{k_{\mathrm{B}}T}\right), \tag{5}$$

where K is a kinetic factor, ΔG^* is the Gibbs free energy required to form a critical nucleus, k_{B} is the Boltzmann constant, and T is the temperature. In the present study of a binary system, homogeneous-heteromolecular nucleation takes place. The Gibbs free energy change of a spherical nucleus bubble is given by

$$\Delta G = \sum_{i=1,2} n_i(\mu_{i,v} - \mu_{i,l}) + 4\pi R_{\mathrm{b}}^2\sigma, \tag{6}$$

where n_i is the number of moles of species i in the bubble, R_{b} is the radius of the bubble, and μ is the chemical potential. The $\Delta G(n_1, n_2)$ plane exhibits a saddle point, which corresponds to the critical vapor bubble. The criteria for determining the saddle point are given by

$$\begin{aligned} &\left(\frac{\partial \Delta \mathrm{G}}{\partial n_1}\right)_{n_2,T,p} = 0,\\ &\left(\frac{\partial \Delta \mathrm{G}}{\partial n_2}\right)_{n_1,T,p} = 0. \end{aligned} \tag{7}$$

Substitution of eq. (7) into eq. (6) yields the Gibbs-Thompson equations for a binary system:

$$\begin{aligned} &(\mu_{1,\mathrm{v}} - \mu_{1,\mathrm{l}}) + \frac{2\sigma\bar{v}_{1,v}}{R_{\mathrm{b}}} = 0,\\ &(\mu_{2,\mathrm{v}} - \mu_{2,\mathrm{l}}) + \frac{2\sigma\bar{v}_{2,v}}{R_{\mathrm{b}}} = 0, \end{aligned} \tag{8}$$

where $\bar{v}_i$ represents the partial molar volume of species i, defined as

$$\bar{v}_i = \left(\frac{\partial V_{\mathrm{b}}}{\partial n_i}\right)_{n_{j\neq i},p,T}, \tag{9}$$

which satisfies the following relation:

$$V_{\mathrm{b}} = \sum_i n_i\bar{v}_i = \frac{4}{3}\pi R_{\mathrm{b}}^3. \tag{10}$$

Using eqs. (5), (8), and (9), the Gibbs free energy change of the critical vapor bubble can be written as

$$\Delta G^* = \frac{4}{3}\pi R_{\mathrm{b}}^2\sigma. \tag{11}$$

The vapor bubble is in mechanical and thermal equilibria with the surrounding liquid. The pressure and temperature inside the vapor bubble can thus be expressed as

$$p_{\mathrm{v}} = p_{\mathrm{l}} + \frac{2\sigma}{R_{\mathrm{b}}}, \tag{12}$$

$$T_{\mathrm{v}} = T_{\mathrm{l}}. \tag{13}$$

The saturation ratio is an input parameter in the present analysis. For a binary mixture, it is defined as the ratio of the mole fraction of secondary species in the liquid phase with respect to the counterpart under saturation conditions:

$$S = \frac{X_{2,\mathrm{l}}}{X_{2,\mathrm{l}}^{\mathrm{sat}}}. \tag{14}$$

For a given pressure, temperature, and saturation ratio, eqs. (8), (12), and (13) can be solved simultaneously to determine the radius, pressure, temperature, and number of molecules in the critical nucleus bubble.

An equation of state is required to calculate various thermodynamic quantities of concern. In the present analysis, the Soave-Redlich-Kwong (SRK) equation of state is employed [31]:

$$p = \frac{\rho R_{\mathrm{u}}T}{W - b\rho} + \frac{a\alpha}{W}\frac{\rho^2}{W + b\rho}, \tag{15}$$

where ρ is the density, R_{u} is the gas constant, and W is the molecular weight of the mixture. The parameters a and b account for attractive and repulsive forces between molecules, respectively. They are calculated using the following mixing rules:

$$\begin{aligned} &a\alpha = \sum_{i=1}^{n}\sum_{j=1}^{n} X_iX_j\left(1 - k_{ij}\right)\sqrt{a_ia_j\alpha_i\alpha_j},\\ &b = \sum_{i=1}^{n} X_ib_i. \end{aligned} \tag{16}$$

The coefficients a_i and b_i are determined from the following universal relationships:

$$\begin{aligned} &a_i = \frac{0.42748R_{\mathrm{u}}^2T_{ci}^2}{p_{ci}},\\ &b_i = \frac{0.08664R_{\mathrm{u}}T_{ci}}{p_{ci}}, \end{aligned} \tag{17}$$

where T_{ci} and p_{ci} are the critical temperature and pressure of species i, respectively. The third parameter, α_i, is given by

$$\alpha_i = \left[1 + S_i\left(1 - \sqrt{T / T_{ci}}\right)\right]^2, \tag{18}$$

with $S_i = 0.48 + 1.574\omega_i - 0.176\omega_i^2$. The surface tension is yet another important property of concern. It is calculated using the Macleod-Sugden correlation [32]:

$$\sigma^{1/4} = \sum_i (P_i)\left[(\rho X_i / W)^{\mathrm{l}} - (\rho X_i / W)^{\mathrm{v}}\right], \tag{19}$$

where P_i is the parachor, which is calculated using experimental data. For oxygen, an empirical correlation for surface tension is available [33].

$$\sigma = \sigma_0\left(1 - \frac{T}{T_c}\right)^p, \tag{20}$$

where the parameters σ_0 and p are equal to 3.95 dyn/cm and 1.255, respectively. The resulting value of parachor is 30. For hydrogen, corresponding-state relation for the surface tension in terms of critical properties and acentric factor is used [32]:

$$\sigma = P_c^{2/3} T_c^{1/3} Q(1 - T / T_c)^{11/9}, \tag{21}$$

where σ is the surface tension in dyn/cm, P_c is the critical pressure in bar, and T_c is the critical temperature in K. The parameter Q is given by

$$Q = \frac{1.86 + 1.18\omega}{19.05}\left[\frac{3.75 + 0.91\omega}{0.291 - 0.08\omega}\right]^{2/3}, \tag{22}$$

where ω is the accentric factor. The resulting value of the parachor of hydrogen is 68.

The kinetic factor is required to calculate the nucleation rate. Theoretical analysis of the kinetics of phase transition was first carried out by Reiss [34] by assuming that each embryo could grow or shrink by acquiring or losing single molecules. The formula was later refined by Stauffer [35], and reported by Zeng and Oxtoby [36]. An expression for the kinetic factor, K, is given by

$$K = N_{\mathrm{A}}\frac{\rho}{W}ABZ, \tag{23}$$

where A is the surface area of the critical nucleus bubble, B is the average growth rate, and Z is the Zeldovich factor. The average growth rate is expressed as

$$\begin{aligned} B &= \frac{j_{n_1} j_{n_2}}{j_{n_1}\sin^2\varphi + j_{n_2}\cos^2\varphi}, \\ \tan\varphi &= s + \left(s^2 + \frac{j_{n_1}}{j_{n_2}}\right)^{1/2}, \\ s &= \frac{D_{22}(j_{n_2} / j_{n_1}) - D_{11}}{2D_{12}}, \\ D_{ij} &= \frac{1}{2}\left(\frac{\partial^2 G}{\partial n_i^{\mathrm{v}} n_j^{\mathrm{v}}}\right)_{T,p}, \end{aligned} \tag{24}$$

where j is the molecular flux. The Zeldovich factor is given by

$$Z = -\frac{D_{11}\cos^2\varphi + 2D_{12}\cos\varphi\sin\varphi + D_{22}\sin^2\varphi}{\left(D_{12}^2 - D_{11}D_{22}\right)^{1/2}}. \tag{25}$$

The theoretical framework is employed to calculate the characteristics of the nucleation of the vapor phase in a liquid droplet. Figure 5 shows the contour plot of the Gibb's free energy change for the oxygen/hydrogen system. The temperature is 110 K, pressure 30 atm, and saturation ratio 5. The saddle point is located near the n_{H_2} axis. As a result, the number of hydrogen molecules in the critical vapor bubble is greater than that of oxygen molecules. For conditions considered in this study, the critical vapor bubble is composed of 17 molecules of oxygen and 110 molecules of hydrogen. The corresponding radius of the bubble is 9.5 Å. It is important to note that the characteristics of the critical vapor bubble depend on the ambient conditions and the saturation ratio.

Figure 6 shows the nucleation rate as a function of the saturation ratio at different pressures. The temperature is

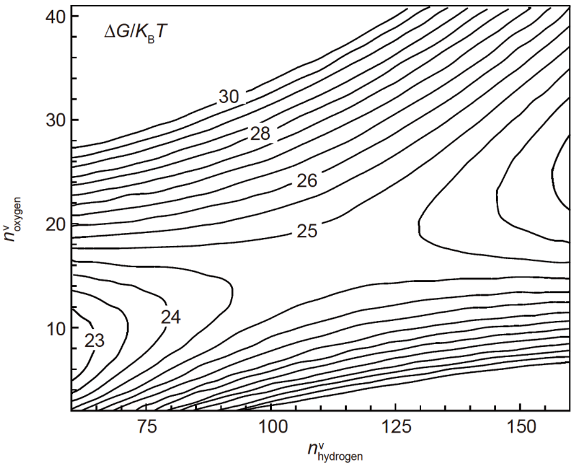

Figure 5 Contour plot of Gibbs free energy in the vicinity of the saddle point; oxygen/hydrogen system, T=110 K, p_{a}=30 atm, S=5.

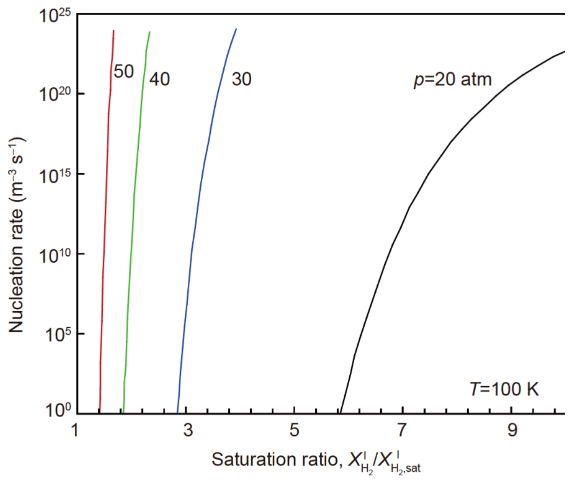

Figure 6 (Color online) Nucleation rate as a function of the saturation ratio at various pressures; oxygen/hydrogen system, T=100 K.

100 K. The nucleation rate is very sensitive to changes in the saturation ratio; it increases by several orders of magnitude when the saturation ratio is increased marginally. At a given pressure, the greater the saturation ratio, the stronger the tendency to nucleation of the vapor phase, and such dependence becomes stronger with increasing pressures. The model also predicts a substantial effect of pressure on the nucleation rate. At a fixed saturation ratio, increasing pressure results in an increase in the nucleation rate by several orders of magnitude. The phenomenon may be attributed to the changes in the composition of the critical vapor bubble, which reduce the surface tension and the energy barrier for vapor nucleation.

Figure 7 shows the saturation ratio corresponding to the threshold nucleation rate as a function of temperature at different pressures. The threshold value of the nucleation rate is arbitrarily chosen to represent the limit between finite rate nucleation and instantaneous nucleation. It is commonly taken as 10^{12} $\mathrm{m^{-3}\ s^{-1}}$ for bubble nucleation [27] and 10^{6} $\mathrm{m^{-3}\ s^{-1}}$ for liquid droplet nucleation. As shown in Figure 6, the nucleation rate increases from 10^{0} to 10^{12} $\mathrm{m^{-3}\ s^{-1}}$ for a slight change in the saturation ratio. The arbitrarily chosen value of the threshold nucleation rate does not significantly influence the results of the present study. The saturation ratio decreases with increasing pressure, from about 6 at 20 atm to 1.4 at 50 atm, for a droplet temperature of 100 K. The reduction of saturation ratio decreases the differences between saturation and superheat conditions. The enthalpy of vaporization thus approaches the saturation counterpart with increasing pressure. This implies that the effect of non-equilibrium conditions on droplet vaporization decreases with increasing pressure.

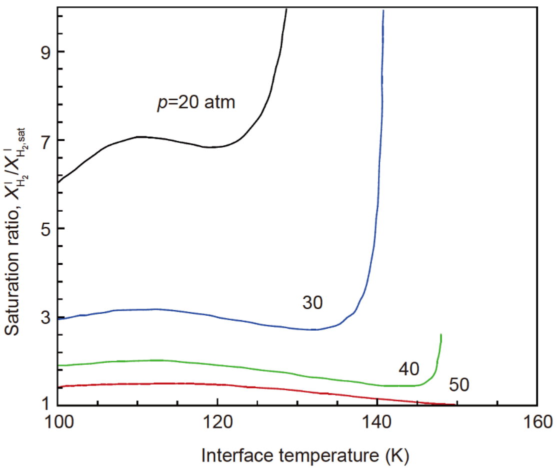

Figure 7 (Color online) Saturation ratio as a function of temperature at various pressures at the kinetic limit; oxygen/hydrogen system.

4 Conclusion

A comprehensive study has been conducted to investigate vaporization of liquid droplets under thermodynamic non-equilibrium conditions over pressures and temperatures typical of those in many liquid-fueled energy conversion systems. The work was performed in two steps. First, the validity of the phase-equilibrium assumption for the gas-liquid interface treatment was examined by means of molecular dynamics theory. An order-of-magnitude analysis was carried out to compare molecular mass flow rates at the interface and the net vaporization rate of the droplet. The isotropic Maxwellian molecular distribution was employed to determine molecular fluxes across the interface. As a specific example, the vaporization of oxygen droplets in gaseous hydrogen was considered. The phase-equilibrium assumption becomes questionable for droplet diameters lower than 10 μm. Ambient pressure and temperature exert limited effects, although the phase-equilibrium assumption holds stronger at relatively high pressures and low temperatures.

The characteristics of droplet vaporization under superheated conditions were then explored following the classical binary homogeneous nucleation theory in conjunction with the SRK equation of state. The nucleation rate was seen to be extremely sensitive to changes in the saturation ratio and pressure of the secondary species; it increases by several orders of magnitude when the saturation ratio or the pressure is increased slightly. In the oxygen/hydrogen system, for example, the kinetic limit of the saturation ratio decreases with increasing pressure, from about 6 at 20 atm to 1.4 at 50 atm for a droplet temperature of 100 K. This leads to the reduced difference between saturation and superheat conditions, and consequently, the influence on non-equilibrium conditions decreases with increasing pressure.

This work was prepared in honor of Academician Xu JianZhong of the Chinese Academy of Sciences on the occasion of his 80th birthday.

1 Sirignano W A. Fluid Dynamics and Transport of Droplets and Sprays. Cambridge: Cambridge University Press, 2010

2 Sirignano W A. Fuel droplet vaporization and spray combustion theory. Prog Energy Combust Sci, 1983, 9: 291–322

3 Faeth G M. Evaporation and combustion of sprays. Prog Energy Combust Sci, 1983, 9: 1–76

4 Sazhin S S. Advanced models of fuel droplet heating and evaporation. Prog Energy Combust Sci, 2006, 32: 162–214

5 Sirignano W A. Advances in droplet array combustion theory and modeling. Prog Energy Combust Sci, 2014, 42: 54–86

6 Sazhin S S. Modelling of fuel droplet heating and evaporation: Recent results and unsolved problems. Fuel, 2017, 196: 69–101

7 Yang V. Modeling of supercritical vaporization, mixing, and combustion processes in liquid-fueled propulsion systems. Proc Combust Inst, 2000, 28: 925–942

8 Hsieh K C, Shuen J S, Yang V. Droplet vaporization in high-pressure environments I: Near critical conditions. Combust Sci Tech, 1991, 76: 111–132

9 Shuen J S, Yang V, Hsiao C C. Combustion of liquid-fuel droplets in

supercritical conditions. Combust Flame, 1992, 89: 299–319
10 Curtis E W, Farrell P V. A numerical study of high-pressure droplet vaporization. Combust Flame, 1992, 90: 85–102
11 Delplanque J P, Sirignano W A. Numerical study of the transient vaporization of an oxygen droplet at sub- and super-critical conditions. Int J Heat Mass Transfer, 1993, 36: 303–314
12 Yang V, Lin N, Shuen J S. Vaporization of liquid oxygen (LOX) droplets in supercritical hydrogen environments. Combust Sci Tech, 1994, 97: 247–270
13 Lafon P, Meng H, Yang V, et al. Vaporization of liquid oxygen (LOX) droplets in hydrogen and water environments under sub- and supercritical conditions. Combust Sci Tech, 2007, 180: 1–26
14 Meng H, Hsiao G C, Yang V, et al. Transport and dynamics of liquid oxygen droplets in supercritical hydrogen streams. J Fluid Mech, 2005, 527: 115–139
15 Birouk M, Abou Al-Sood M M. Droplet evaporation in a turbulent high-pressure freestream: A numerical study. Int J Thermal Sci, 2010, 49: 264–271
16 Meng H, Yang V. Vaporization of two liquid oxygen (LOX) droplets in tandem in convective hydrogen streams at supercritical pressures. Int J Heat Mass Transfer, 2014, 68: 500–508
17 Kuo K K. Principles of Combustion. New Jersey: John Wiley & Sons, Inc., 2005
18 Aggarwal S K, Sirignano W A, Tong A Y. A comparison of vaporization models in spray calculations. AIAA J, 1984, 22: 1448–1457
19 Abramzon B, Sirignano W A. Droplet vaporization model for spray combustion calculations. Int J Heat Mass Transfer, 1989, 32: 1605–1618
20 Miller R S, Harstad K, Bellan J. Evaluation of equilibrium and non-equilibrium evaporation models for many-droplet gas-liquid flow simulations. Int J Multiph Flow, 1998, 24: 1025–1055
21 Dahms R N, Oefelein J C. Non-equilibrium gas-liquid interface dynamics in high-pressure liquid injection systems. Proc Combust Inst, 2015, 35: 1587–1594
22 Sazhin S S, Shishkova I N, Kryukov A P, et al. Evaporation of droplets into a background gas: Kinetic modelling. Int J Heat Mass Transfer, 2007, 50: 2675–2691
23 Sazhin S S, Shishkova I N, Al Qubeissi M. A self-consistent kinetic model for droplet heating and evaporation. Int J Heat Mass Transfer, 2016, 93: 1206–1217
24 Librovich B V, Nowakowski A F, Nicolleau F C G A, et al. Non-equilibrium evaporation/condensation model. Int J Appl Mech, 2017, 09: 1750111
25 Xie J F, Sazhin S S, Cao B Y. Molecular dynamics study of the processes in the vicinity of the *n*-dodecane vapour/liquid interface. Phys Fluids, 2011, 23: 112104
26 Xiao G, Luo K H, Ma X, et al. A molecular dynamics study of fuel droplet evaporation in sub- and supercritical conditions. Proc Combust Inst, 2019, 37: 3219–3227
27 Carey V P. Liquid Vapor Phase Change Phenomena: An Introduction to the Thermophysics of Vaporization and Condensation Processes in Heat Transfer Equipment. Florida: CRC Press, 2018
28 Cao B Y, Xie J F, Sazhin S S. Molecular dynamics study on evaporation and condensation of *n*-dodecane at liquid-vapor phase equilibria. J Chem Phys, 2011, 134: 164309
29 Liang Z, Biben T, Keblinski P. Molecular simulation of steady-state evaporation and condensation: Validity of the Schrage relationships. Int J Heat Mass Transfer, 2017, 114: 105–114
30 Seinfeld J H, Pandis S N. Atmospheric Chemistry and Physics: From Air Pollution to Climate Change. New Jersey: John Wiley & Sons, Inc., 2016
31 Meng H, Yang V. A unified treatment of general fluid thermodynamics and its application to a preconditioning scheme. J Comput Phys, 2003, 189: 277–304
32 Reid R C, Prausnitz J M, Poling B E. The Properties of Gases and Liquids. New York: McGraw-Hill Companies, Inc., 1987
33 Kai T, Nomoto H, Deguchi M, et al. Surface tension of ternary mixtures of nitrogen, oxygen, and argon. J Chem Eng Data, 1994, 39: 499–501
34 Reiss H. The kinetics of phase transitions in binary systems. J Chem Phys, 1950, 18: 840–848
35 Stauffer D. Kinetic theory of two-component (“hetero-molecular”) nucleation and condensation. J Aerosol Sci, 1976, 7: 319–333
36 Zeng X C, Oxtoby D. Binary homogeneous nucleation theory for the gas-liquid transition: A nonclassical approach. J Chem Phys, 1991, 95: 5940–5947